INTERNATIONAL JOURNAL OF INTEGRATED ENGINEERING
ISSN: 2229-838X e-ISSN: 2600-7916

IJIE

Vol. 16 No. 7 (2024) 266-279
https://publisher.uthm.edu.my/ojs/index.php/ijie

Optimizing Hydrophilicity in NiO/Graphene Composites Via Stearic Acid Treatment for Humidity-to-Energy Applications

Nurul Syafiqah Mohamed Mustakim[1], Dayana Kamaruzaman[1,2], A Shamsul Rahimi A Subki[3], Mohd Hanapiah Abdullah[4], Mohd Firdaus Malek[5], Norfarariyanti Parimon[6], Mohd Khairul Ahmad[7], Suriani Abu Bakar[8], Nagamalai Vasimalai[9], Mohamad Hafiz Mamat[1]*

[1] *NANO-ElecTronic Centre (NET), School of Electrical Engineering, College of Engineering, Universiti Teknologi MARA, 40450 Shah Alam, Selangor, MALAYSIA*
[2] *School of Electrical Engineering, College of Engineering, Universiti Teknologi MARA, Cawangan Terengganu, Kampus Dungun, 23000 Dungun, Terengganu, MALAYSIA*
[3] *Faculty of Electronics Engineering and Computer Technology (FTKEK), Universiti Teknikal Malaysia Melaka, Hang Tuah Jaya, 76100 Durian Tunggal, Melaka, MALAYSIA*
[4] *Centre for Electrical Engineering Studies, Universiti Teknologi MARA, Cawangan Pulau Pinang, 13500 Permatang Pauh, Pulau Pinang, MALAYSIA*
[5] *NANO-SciTech Lab (NST), Centre for Functional Materials and Nanotechnology (CFMN), Institute of Science (IOS), Universiti Teknologi MARA, 40450, Shah Alam, Selangor, MALAYSIA*
[6] *Faculty of Engineering Universiti Malaysia Sabah, 88400 Kota Kinabalu, Sabah, MALAYSIA*
[7] *Microelectronic and Nanotechnology–Shamsuddin Research Centre (MiNT-SRC), Faculty of Electrical and Electronic Engineering, Universiti Tun Hussein Onn Malaysia, Batu Pahat Johor, Parit Raja, 86400, MALAYSIA*
[8] *Nanotechnology Research Centre, Faculty of Science and Mathematics, Universiti Pendidikan Sultan Idris, 35900 Tanjung Malim, MALAYSIA*
[9] *School of Physical and Chemical Sciences, B.S. Abdur Rahman Crescent Institute of Science & Technology, Vandalur, Chennai 600 048, INDIA*

*Corresponding Author: mhmamat@uitm.edu.my
DOI: https://doi.org/10.30880/ijie.2024.16.07.024

Article Info

Received: 27 June 2024
Accepted: 17 November 2024
Available online: 31 December 2024

Keywords

Humidity-to-energy, Hydroscopic material, Renewable energy, Stearic acid treatment

Abstract

Converting water molecules into energy, this research field has garnered significant attention, yet it is still in its early stages of exploration. The main challenge in humidity-to-energy development is the effectiveness of material in water absorption. This article presents a study on surface modification through stearic acid treatment aimed at optimizing the hydrophilicity of hygroscopic material, thereby improving humidity energy harvesting performance. Here, we successfully synthesized a novel NiO/Graphene on cellulose substrate (NiO/Gr/cellulose) as the hygroscopic material using the sonicated solution immersion method. A humidity-to-energy device was fabricated by utilizing the NiO/Gr/cellulose, yielding an output voltage of 2.26 mV, a current density of 0.18 nA/cm^2, and a power output of 0.51 pW at 75% relative humidity. This research highlights the potential of NiO/Gr/cellulose with sufficient hydrophilicity as a promising hygroscopic material, offering significant future prospects in humidity energy harvesting technology.

1. Introduction

Renewable energy (RE) is currently a hot topic in the research field worldwide. Examples of RE include photovoltaic cells [1-5], biofuels [6-7], and wind power generation [8,9]. However, these sources of RE face challenges. Solar energy, for instance, cannot solely provide electricity as the sun is not visible throughout the day, and the initial costs of solar panel installation are very high [3]. Biofuel RE requires large-scale cultivation of microalgae, which consumes significant water, nitrogen, and phosphorus, and may even generate greenhouse gases, leading to climate issues [6]. Wind energy, while popular, is hindered by the unpredictable nature of wind, difficulties in forecasting, and the inability to store it, along with the expenses of operation and maintenance [10-11].

Humidity-to-energy technology has emerged as a potential major alternative energy source. Humidity, an abundant resource consisting of water molecules in vapor state, can be harnessed to produce green electricity. Initial studies on energy harvesting from humidity were reported as early as 2013, where electricity was generated using bacterial spores reacting to changes in humidity [12]. Subsequent reports in 2014 introduced evaporation-driven engines that successfully generated electrical power from water evaporation due to changes in surrounding humidity [13]. Further research in 2015 demonstrated humidity gradient-based power generators utilizing graphene oxide [14]. These pioneering works specifically focused on converting humidity into electricity, opening new opportunities for RE research and development.

Hygroscopic materials, also known as humidity-absorbing materials, are key components in humidity-to-energy conversion technology. This technology operates based on hydration-induced ionization effects. When hygroscopic materials are placed between two metal electrodes and exposed to atmospheric humidity, water molecules are absorbed, leading to subsequent hydration and the production of free charge carriers through ionization effect [15]. The gradient configuration within hygroscopic materials induces the diffusion of charge carriers, creating an electric potential between the electrodes and initiating current flow [16]. Thus, precise structural control and surface modification of hygroscopic materials are crucial, affecting their hydrophilicity, which plays a vital role in facilitating water molecule adsorption onto the material surface. As the working principle of humidity-to-energy been discussed, noted that the adsorption process is pivotal for converting atmospheric humidity into usable energy. Materials with good hydrophilicity tend to exhibit better water adsorption properties, contributing to the overall effectiveness of humidity-based energy harvesting devices [17-18]. Ensuring sufficient hydrophilicity is essential to optimize performance in humidity-to-energy technology. Reported that the hydrophilicity of material can be controlled by the functionalization process of stearic acid (SA) treatment [19].

Surface wettability, typically defined by the water contact angle (θ_{CA}) between a water droplet and a solid surface, categorizes surfaces into four main properties: super-hydrophilic (≤ 5°), hydrophilic (≤ 90°), hydrophobic (≥ 90°), and super-hydrophobic (≥ 150°) [20-21]. A strong hydrophilic surface, characterized by high affinity for water and high surface energy, results in water spreading well on the material, leading to a low θ_{CA}. As reported, surface properties are an important factor that influences surface wettability [22].

While NiO nanoparticles have a broad bandgap of 3.6 - 4.0 eV and are inexpensive as well as highly stable conductive materials, they are widely used in numerous of applications [23-26]. Conversely, graphene (Gr) is renowned for its high electrical and thermal conductivities, as well as its precise control over functionalization properties [27]. Both NiO and Gr have been recognized as notable candidates for a range of applications, including photovoltaic cells [28,29], sensors [30-34], thin film transistors [35-38], and more. A number of studies on NiO/Gr composite employing diverse synthesis methods and applications are shown in Table 1. Based on these studies, it is demonstrated that the NiO/Gr composition exhibits long-term stability and durability under various conditions. In this study, a novel NiO/Gr composite will be utilized as the hygroscopic material in the humidity-based energy harvesting device. Essentially, this hygroscopic material will function as a trap for positive ions. The zeta potentials of NiO and Gr have been reported to be approximately -35 mV and -33 mV, respectively [39]. These negative zeta potentials attract positive ions, primarily H+ ions, to the surfaces of NiO and Gr. The negative zeta potential arises from surface hydroxyl groups, which structurally and chemically undergo an association-dissociation mechanism leading to O-rich surface formation. A surface modification strategy for NiO/Gr hygroscopic nanomaterials represents a beneficial approach considering the zeta potential, which will stimulate ion movement for the generation of electric fields and currents, thus enhancing the overall performance of humidity-to-energy systems.

Int. Journal of Integrated Engineering Vol. 16 No. 7 (2024) p. 266-279

Table 1 *Comparison of studies on NiO/Gr composite employing different synthesis methods and applications*

Material	Application	Composition	Method	Study outcome	Ref.
NiO@NiS@G	Dye-sensitized solar cell	45 mg of GO dispersion	Hydrothermal	Efficiency: 2.10%	[40]
NiO-GO	Perovskite solar cells under humidity condition	Different GO mass ratios (0.0 to 2.0 wt%)	Solution immersion	Efficiency: 20.8%	[41]
NiO/G	Pseudocapacitor electrodes	0.5 g Ni $(NO_3)_2$, $6H_2O$ in 20 mL GO	Hydrothermal	Power density: 2800 Wkg^{-1}	[42]
Porous graphene-NiO (PGNO)	Supercapacitors	Different wt.% GO	Solvothermal	Current density: 8 A g^{-1}	[43]
NiO_x/ Vertical graphene nanosheets (VGN)	Electrochemical capacitor	Different NiO deposition time	DC sputtering	Capacitance value: 0.15 mF cm^{-2}	[44]
rGO/NiO	Gas sensor under high humidity	Different wt.% GO	Microwave-assisted hydrothermal	Highest response: 61.51%	[45]
Ni-NiO@Gr	Wastewater treatment of textile industries	Variation in pH, temperature, initial concentration of CV dye, and contact period	Single step	Maximum adsorption capacity increased from 1028 to 1230 mg/g	[46]
NiO/Graphene	Humidity-to-energy	Stearic acids treatment	Sonicated solution immersion	Output voltage: 2.26 mV, current density: 0.18 nA/cm^2	This study

While humidity-based energy-harvesting technologies have the potential to be self-sufficient energy systems, the development of materials for humidity-to-energy conversion is still in its preliminary phase and progressing slowly. Table 2 shows several studies on studies on humidity-to-energy conversion. Since there have been only a few successful reports in this particular field, the mechanism underlying the energy conversion process from humidity is not thoroughly studied. The primary issues that this technology frequently faces are its low energy productivity also its complicated construction procedures [47-48].

Table 2 *Comparison of output performance based on several studies on humidity-to-energy conversion*

Material	Electrical output	Method	Aim of study	Ref.
MXene ($Ti_3C_2T_x$) aerogel	24.8 $\mu W/cm^2$	Gelation process	Moisture-driven energy generators with a bilayered architecture	[49]
Protein nanowires	2.5 $\mu W/cm^2$	Bacterial Culture Preparation	Device performance with whole-cell and without the protein nanowires	[50]
Robust porous carbon film	8.1 $\mu W/cm^3$	Electrodeposition	Utilization of all-printed porous carbon film in power generation	[51]
TiO_2 nanowire	4 $\mu W/cm^2$	Layer-by-layer assembly	Power generation based on TiO_2 nanowire networks containing 3D nanochannels structure	[52]
Porous Graphene oxide membrane	2.02 $\mu W/cm^2$	Directionally induced thermal reduction	Utilization asymmetric porous graphene oxide membrane to produce power output	[53]

To our knowledge, no reports specifically address the effect of material hydrophilicity on the humidity-to-energy performance of NiO/Gr when used as hygroscopic materials. Here, we synthesized NiO/Gr using a straightforward sonicated solution immersion method and deposited the hygroscopic material onto a cellulose substrate for the fabrication of the humidity-to-energy device. The novel NiO/Gr on cellulose substrate (NiO/Gr/cellulose) then underwent SA treatment for surface modification under specific SA concentrations, immersion temperatures, and times. Our objective is to achieve improved hydrophilic NiO/Gr hygroscopic materials via SA treatment, thereby yielding outstanding results in the development of humidity-to-energy technology.

2. Methodology

2.1 Synthesis of NiO/Gr Nanostructured Powder

Nickel nitrate hexahydrate (Ni $(NO_3)_2 \cdot 6H_2O$) (Sigma-Aldrich), graphene nanoplatelets (99.98%, Techinstro) and hexamethylenetetramine (HMT) ($C_6H_{12}N_4$, 99.0%, Sigma-Aldrich) were used as the precursor materials and stabilizer, respectively. NiO/Gr nanomaterials sample was synthesized using sonicated solution immersion method. Initially, disperse 0.2 M of Ni $(NO_3)_2 \cdot 6H_2O$, 0.2 M of HMT and 1.0 weight percent (wt.%) of graphene nanoplatelets into deionized water (DI water). To ensure thorough mixing, the solution underwent sonication in an ultrasonic bath (Hwashin Technology Powersonic 405) for 1 hour, followed by stirring at 500 rpm for an additional hour. After that, the homogenous mixture was poured into a 100 mL Schott bottle (DURAN), tightly closed, and immersed for an hour at 75°C in a water bath (Memmert). After immersion, the produced precipitates were collected and filtered using Whatman Qualitative Grade 1 filter paper (diameter 110 mm). The obtained nanomaterials were dried overnight at 36°C to eliminate the remaining water molecules. Subsequently, to achieve better crystallinity, the dried sample was then annealed in a chamber furnace chamber (Protherm) at 500°C for one hour in an ambient environment. The procedure depicted is illustrated in Fig. 1.

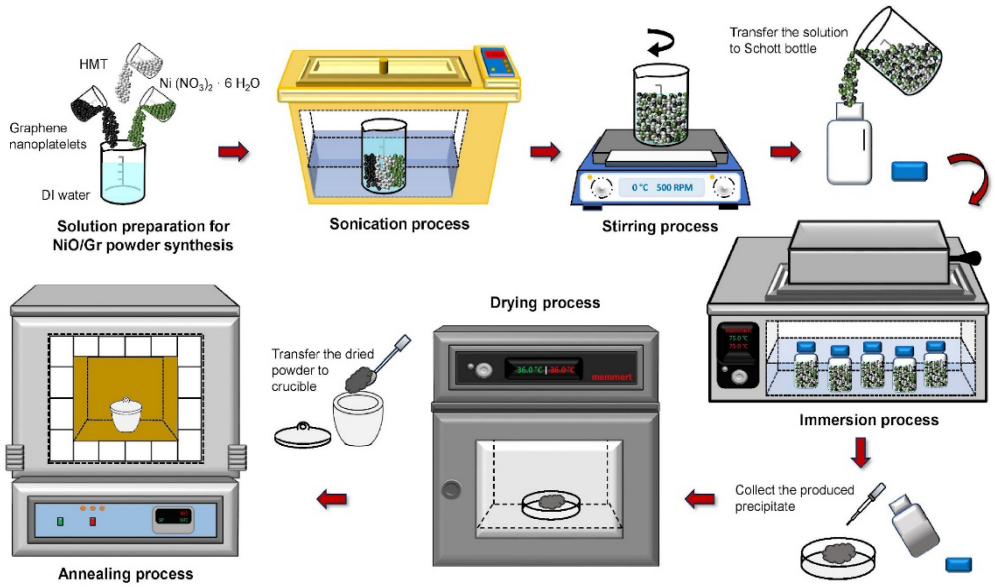

Fig. 1 *Synthesis of the NiO/Gr nanomaterials through the ultrasonicated solution immersion method*

2.2 Stearic Acid Treatment

To improve hydrophilic properties, the NiO/Gr samples underwent stearic acid treatment at certain concentrations, immersion temperatures, and durations, as illustrated in Fig. 2. SA (95%, Sigma-Aldrich) was dissolved in ethanol (99.8%, SYSTERM) at 2 wt.%. The solution was then sonicated for 10 minutes. After adding the prepared NiO/Gr powder, the mixture was stirred at 300 rpm at temperatures of 60°C for 6 hours (hrs). Afterward, the solution was filtered and dried overnight at 36°C.

Int. Journal of Integrated Engineering Vol. 16 No. 7 (2024) p. 266-279

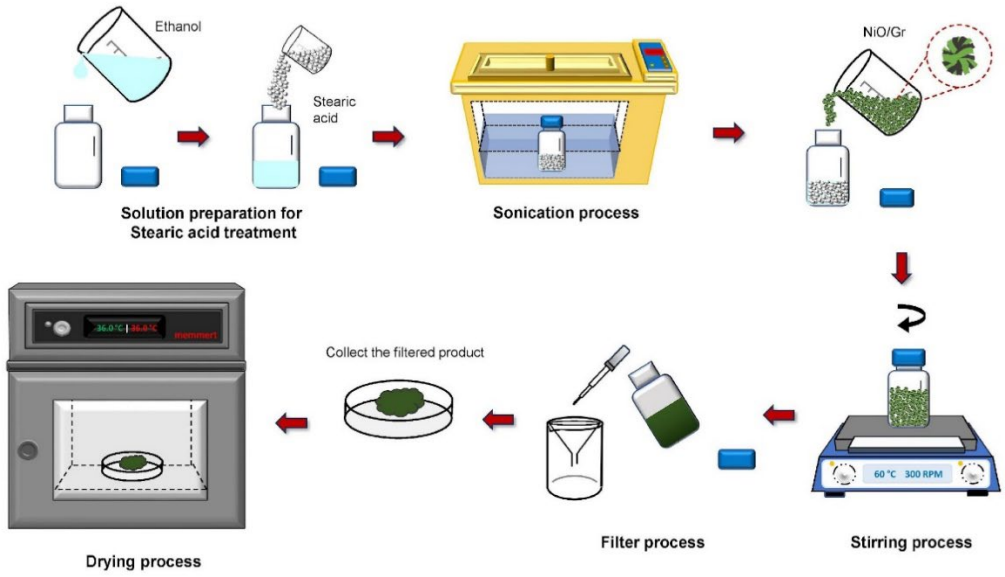

Fig. 2 *Stearic acid treatment on NiO/Gr*

2.3 Fabrication of Humidity-to-Energy Device

1 g of SA-treated NiO/Gr nanostructured powder was dispersed in 15 mL of transparent adhesive liquid (Chunbe 6603), serving as a binder. The resulting paste was labelled as NiO/Gr paste. Using cellulose filter paper (Whatman Qualitative Grade 1, diameter 110 mm) as a substrate, a shaped pattern measuring 15 mm × 15 mm was prepared. Subsequently, the NiO/Gr paste was applied using the doctor blade technique to create a uniform thin coating of hygroscopic material on the cellulose substrate. Following this, the deposited hygroscopic layer was left to dry on a hot plate at 90°C for 1 hour before applying the working electrode, measuring 5 mm × 5 mm in contact size, onto the film. The gap between the contacts was measured at 5 mm. To prepare the working electrode, commercial silver (Ag) conductive paste (Mechanic, MCN-DJ002) was applied onto the hygroscopic layer in accordance with the patterned cellulose substrate as illustrated in Fig. 3.

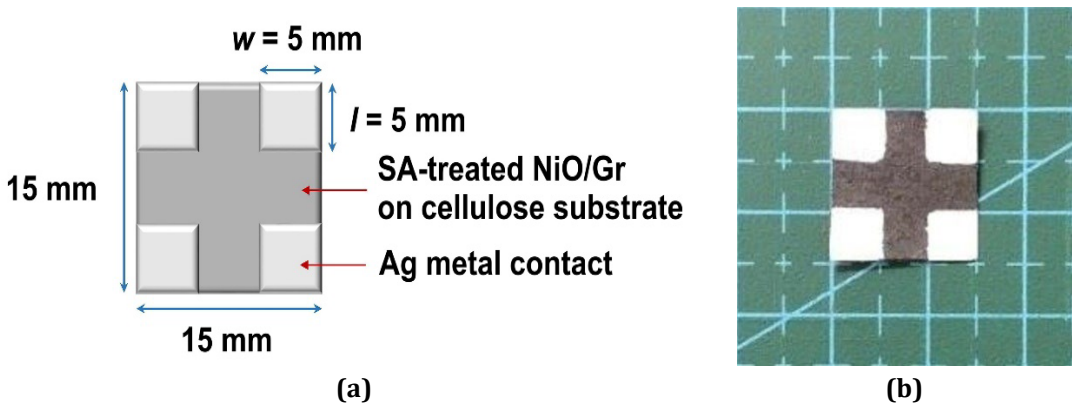

Fig. 3 *(a) The structural layout; and (b) image of the fabricated SA-treated NiO/Gr-based humidity-to-energy device*

2.4 Characterizations

The morphological studies and the elemental composition analyses for the SA treated-NiO/Gr nanomaterials were conducted using field emission scanning electron microscopy (FE-SEM; JEOL JSM-7600F; 15 kV of energy operating voltage) and scanning electron microscopy (SEM) equipped with energy dispersive X-ray spectroscopy (EDX; Scanning range of 0 - 10 keV) (Hitachi, SU-3500). Platinum (Pt) coatings (10 nm thick; auto fine coater, JEOL JFC-1600) were applied to the sample before the EDX measurements in order to minimize charging in the SEM images. Using Cu-Kα1 radiation (λ = 1.5406 Å) in the 2θ range from 20° to 90°, X-ray diffraction (XRD; Rigaku, UltimaIV) was used to characterize the crystallinity and phase formation. The water contact angle (WCA) of NiO on cellulose substrate was investigated using wafer surface analysis system (VCA-3000, AST product, Inc). The

chemical group identification was carried out by Fourier transform infrared spectroscopy (FTIR) on untreated and treated samples using a Spectrometer Frontier (Perkin Elmer, Spectrum One). Each sample scanned in attenuated total reflection (ATR) from 4000 to 350 cm^{-1} wavenumbers. To investigate the device's response to humidity and its performance, measurements were conducted in a bench-top temperature and humidity chamber (ESPEC-SH261) equipped with a current-voltage-time measurement system (I-V-t;Keithley 2400) at 25°C.

3. Result

3.1 Structural Characterizations – XRD and FTIR

Fig. 4 shows the XRD patterns of untreated and SA-treated NiO/Gr nanostructure. The observed peaks matching well with the reported (PDF card No. 01-071-4750) data of NiO, (PDF card No. 004-0850) data of nickel, (PDF card No. 041-1487) data of graphite, (PDF card 056-1718) data of cellulose and (PDF card No. 038-1923) data of stearic acid. The diffraction peaks at 37.04° were indexed to the (1 1 1) corresponding to NiO, respectively. Meanwhile, the peaks at 44.51° and 51.85° were indexed to the Ni (1 1 1) and Ni (2 0 0) planes of nickel, respectively. The diffraction peaks which are relevant for Gr are in the positions of 26.38° and 54.54° corresponding to the planes of *(0 0 2) and *(0 0 4), respectively. The XRD patterns clearly exhibit the planes of ● (2 0 0) and ● (2 3 1) at diffraction peak 22.36° and 43.92°, respectively, corresponding to cellulose. For stearic acid, diffraction peaks at 21.63° and 24.18° corresponding to ♦ (3 1 1) and ♦ (6 0 2), respectively.

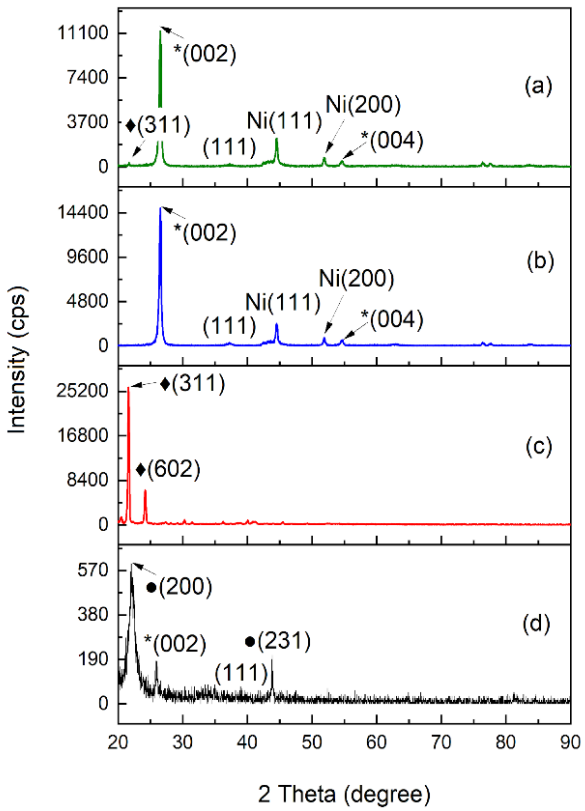

Fig. 4 *XRD pattern for (a) SA-treated NiO/Gr; (b) untreated NiO/Gr; (c) pure SA; and (d) SA treated NiO/Gr on cellulose substrate*

From XRD results, the crystallite size (D) of NiO/Gr nanostructures calculated from (1 1 1) peak of NiO by using Debye–Scherrer equation [54]:

$$D = \frac{K\lambda}{\beta \cos\theta} \quad (1)$$

where K represents a constant, given as 0.9, while λ is the XRD's X-ray wavelength (λ = 1.5418 Å), θ is the diffraction angle and β refers to full width at the half maximum (FWHM), which correlates with the diffraction broadening due to the dimensions of the crystallite. The findings demonstrated a decrease in D from 8.65 nm to 5.31 nm following SA treatment, as presented in Table 3. Additionally, variations in FWHM values and shifts in position were noted pre- and post-SA treatment, suggesting structural alterations resulting from the treatment.

Int. Journal of Integrated Engineering Vol. 16 No. 7 (2024) p. 266-279

Table 3 *The crystallite size of NiO/Gr nanostructures calculated using the Debye-Scherrer formula*

Sample	FWHM, β (rad.)	Lattice parameter, a (nm)	Interplanar spacing, d (nm)	Unit Cell Volume, V (nm^3)	Crystallite size, D (nm)
Untreated NiO/Gr	0.017	0.419	0.242	0.073	8.65
SA-treated NiO/Gr	0.028	0.419	0.242	0.074	5.31

Based on the FTIR spectra in Fig. 5, there are peaks at 2913.45 cm^{-1} and 2847.80 cm^{-1} that are related to the asymmetric and symmetric stretching of CH_2 groups of pure SA, respectively [55]. The peak at 1699.18 cm^{-1} is related to stretching vibration of carbonyl double bond, meanwhile, peaks at 1462.95 cm^{-1}, 1429.48 cm^{-1} and 1411.20 cm^{-1} are related to bending vibrations of CH_2 groups. For SA-treated NiO, new peak was observed at 2345.59 cm^{-1} attributed to asymmetric stretching vibrations mode of the CO_2 molecule presented from the ambience [56]. The absorption band at 548.26 cm^{-1} have slightly shifted to higher wavenumber at 566.71 cm^{-1}, indicating that SA is bonded to the surface of the NiO nanoparticles. The peak at 1297.11 cm^{-1} and 940.51 cm^{-1} were correlated to the bending and rocking vibration, respectively, of the CH_2 functional group in pure SA. However, the presence of this group on the SA treated NiO surface leads to unreacted SA, thus no peaks were observed at both bands [57].

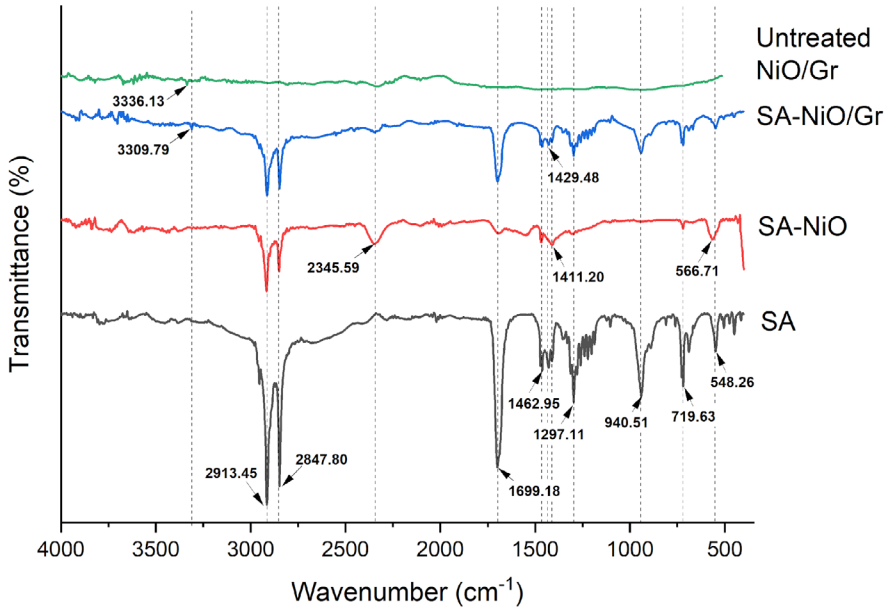

Fig. 5 *FTIR spectra for pure SA, SA-treated NiO, SA-treated NiO/Gr and untreated NiO/G*

For NiO/Gr, a new peak at 3336.13 cm^{-1} is due to presence of stretching vibrations of OH functional group which originated from the interactions on the Gr surface. After SA treatment, the absorption band was observed shifted to lower wavenumber of 3309.70 cm^{-1}, which originates from the functionalization process [58].

3.2 Surface Morphology – FESEM and EDX

For Fig. 6 presents the FESEM images of NiO/Gr morphologies pre- and post-SA treatment. Fig. 6(a) and (b) display the surface of NiO/Gr before SA treatment, revealing nanostructured aggregates, with an average diameter (d_x) range of 60.6 – 172.4 nm. Fig. 6 (c) and (d) illustrate significant changes after treating the NiO/Gr with SA, resulting layered and overlapping surface which resembled the arrangement of scales on fish with agglomerated small nanoparticles, with an average d_x of 52.7 -105.9 nm. Fig. 6 (e) shows the image of SA-treated NiO/Gr deposited on cellulose substrate. As observed, the treated NiO/Gr were attached well on the cellulose fibers. The EDX of the NiO/Gr nanostructure are shown in Fig. 6 (f) which confirms the presence of carbon (C), oxygen (O), and nickel (Ni) elements, with peaks appearing between 0 to 10 keV. No other elements are detected in the EDX spectra, indicating that these results align with the XRD spectra findings.

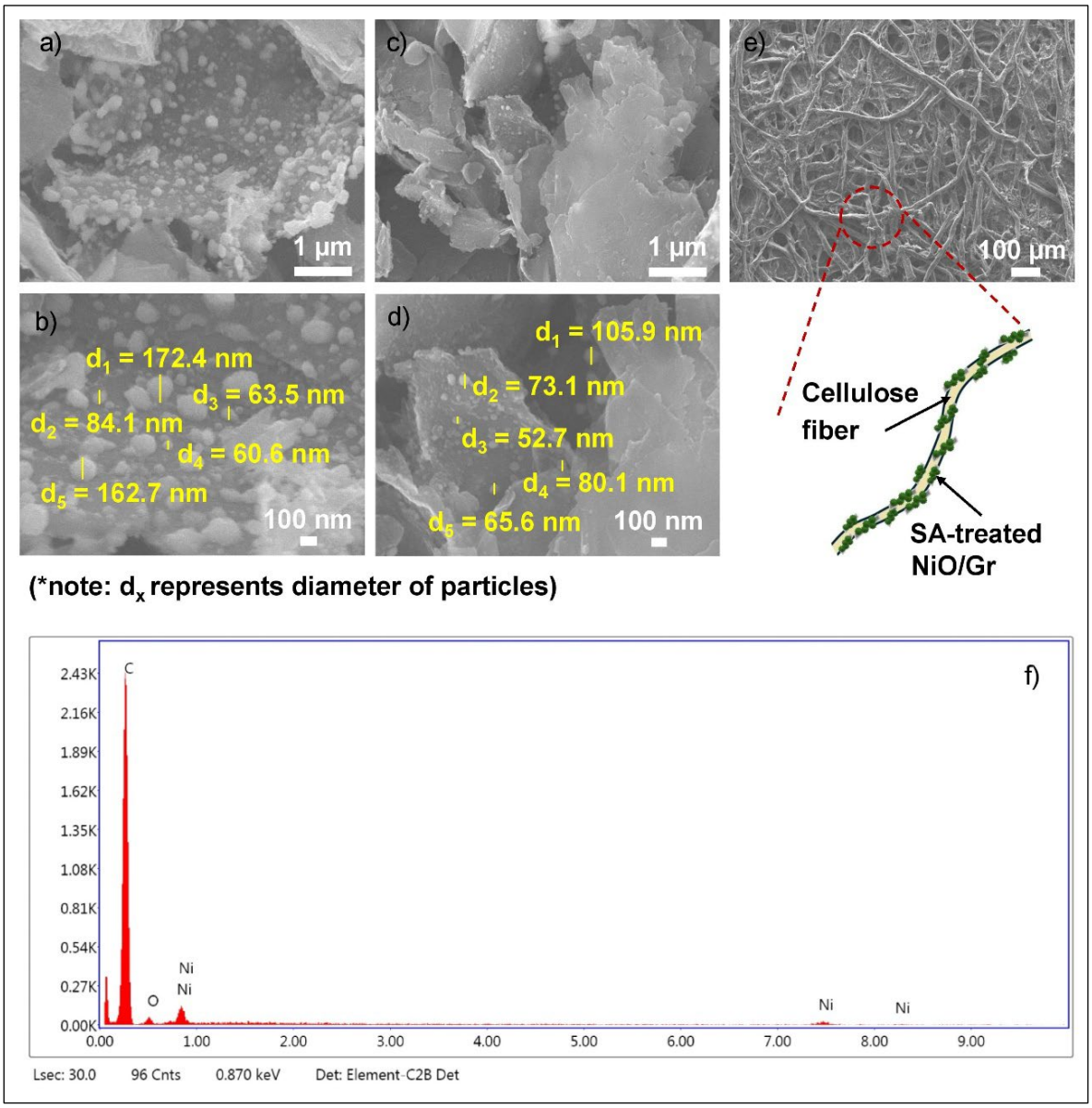

Fig. 6 *FESEM images of untreated NiO/Gr (a) x 20,000 magnification, 15 kV applied voltage; (b) x 50,000 magnification, 15 kV applied voltage. FESEM images of SA-treated NiO/Gr; (c) x 20,000 magnification, 15 kV applied voltage; (d) x 50,000 magnification, 15 kV applied voltage; (e) Illustration of SA-treated NiO/Gr on cellulose substrate and (f) EDX peaks with analytic elemental composition of NiO/Gr nanocomposite (inset)*

3.3 Hydrophilicity Properties – WCA

Fig. 7 shows images of water droplets on the surface of substrate. One way to determine the surfaces' wettability is by estimating the sample's corresponding surface energy by analyzing their θ_{CA} measurements. The surface energy can be calculated using simplified Fowkes-Girifalco-Good-Young theory [59]:

$$\gamma_s^d = \frac{1}{4}\gamma_l(\cos\theta_{CA} + 1) \quad (2)$$

$\gamma^d{}_s$ is denoted as the dispersive portions of the surface tension for the solid surfaces and assuming $\gamma_l\gamma_l$ is approximately equal to the testing liquid used which is the nonpolar liquid deionized water with a surface tension of 72.8 mJ/m^2. The calculated surface energy for each sample is shown in Table 4.

Int. Journal of Integrated Engineering Vol. 16 No. 7 (2024) p. 266-279

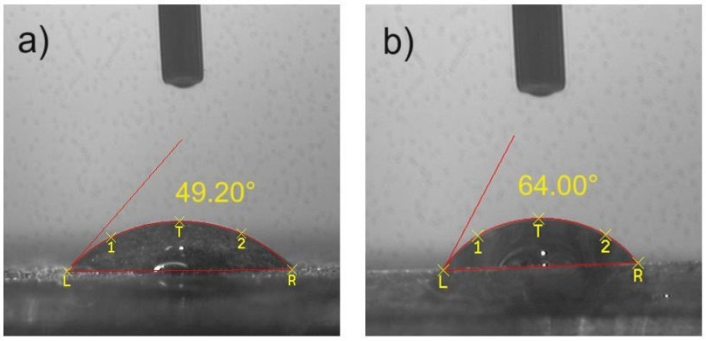

Fig. 7 *Contact angle measurement (a) untreated NiO/Gr; (b) SA-treated NiO/Gr*

Table 4 *Water contact angle and surface energy of untreated NiO/Gr and SA-treated NiO/Gr*

NiO/Gr	Water contact angle (°)	Surface energy (mL/m^2)
Untreated	49.20	30.09
SA-treated	64.00	26.18

The results clearly indicate that SA-treated NiO/Gr/cellulose has higher θ_{CA} between the water droplet and substrate surface compared to the untreated substrate. However, the θ_{CA} of the SA-treated sample which is 64.00° which is still in hydrophilic nature. From the calculations, the surface energy obtained for SA-treated NiO/Gr/cellulose substrate is 26.18 mJ/m^2 which is lower than the untreated sample. Generally, high surface energy means a strong molecular attraction which leads to easier to form bonds, the water spreads on the material and thus the θ_{CA} become low, whereas low surface energy means vice versa [22]. Notably, the surface's wettability behavior correlates closely with the surface morphology of the sample. Surface modification from the SA treatment allows more SA molecules to attach onto the sample surface, therefore forming a denser and well-arranged self-assembled monolayer (SAM). This is aligned with the FESEM images that show the layered and overlapping surface of SA-treated substrate which tend toward rougher surface. According to reports, larger surface roughness could indicate poor hydrophilicity where large amount of air trapped in the gap of agglomerated nanostructures formation [59,60].

4. Electrical Properties – I-V Measurements

Surface wettability of a sample has a significant impact which affects the performance of the humidity-to-energy device. Hydrophilicity of material will influence output voltage of the device. Therefore, it is crucial to undergo SA treatment for surface modification in order to determine the optimum hydrophilicity properties. To evaluate the device's response towards humidity and its operational efficiency, measurements were conducted with zero bias. The humidity-to-energy performance of the fabricated devices was presented in Table 5. Fig. 8. (a) show the voltage versus time at 75% of relative humidity (RH) while Fig. 8 (b) and (c) show current versus time from 40% RH to 90% RH for untreated and SA-treated devices, respectively.

Table 5 *The humidity-to-energy performance of fabricated devices*

Sample	Area, A (cm^2)	RH (%)	Resistance, R (Ω)	Output voltage, V (V)	Current density, J (A/cm^2)	Power, P (W)
Untreated	1.25	75	10M	1.39×10^{-4}	1.11×10^{-11}	1.92×10^{-15}
SA-treated	1.25	75	10 M	2.26×10^{-3}	1.81×10^{-10}	5.09×10^{-13}

From the result, it is confirmed that the humidity response performance of the NiO/Gr/cellulose humidity-to-energy device improved with the SA treatment process. At 75% RH, noted that the output voltage of the SA-treated device produced was up to 2.26 mV with current density of 1.81×10^{-10} A/cm^2 which is better than untreated device. This is because the composite hygroscopic material with SA treatment is able to trap more water molecules at high RH and resulting in significant voltage production [17]. The response and recovery time of the humidity-to-energy device is known as the time needed for the total output voltage change to reach 90% during both absorption (40%–90% RH) and desorption (90%–40% RH). From the study, when the RH achieved 90%, untreated devices yielded the highest current output of 5.03×10^{-10} A at 593 s, while the SA-treated device

achieved the highest current output of 2.27 × 10^{-09} A at 566 s. On the other hand, untreated devices took about 607 s for recovery time. The SA-treated device took slightly longer time, which is 633 s. Regardless of the specifics, both humidity-to-energy devices still provide excellent responses and recovery during the humidity changes.

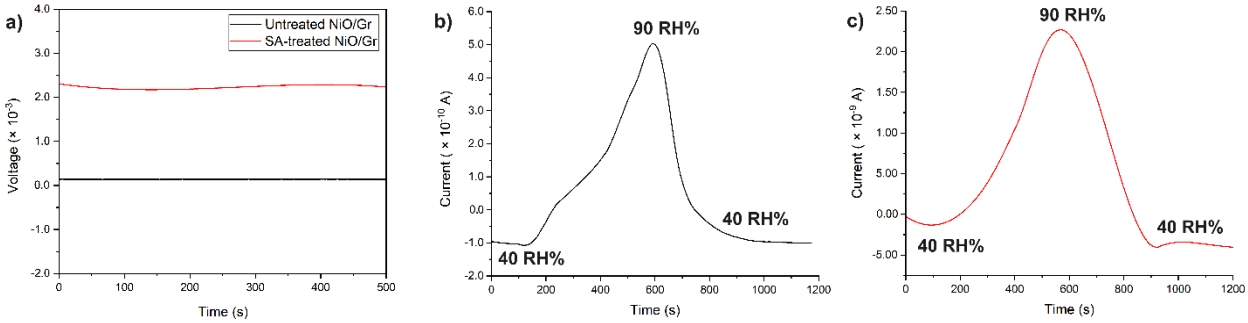

Fig. 8 *Humidity response of (a) untreated and SA-treated NiO/Gr humidity-to-energy device at 75% RH with 0 A bias; (b) untreated; and (c) SA-treated humidity-to-energy device from 40% to 90% RH with 0 V bias*

5. Conclusion

In conclusion, this study confirms that surface treatment with SA on the hygroscopic material of NiO/Gr which than deposited on cellulose substrate helps enhance humidity-to-energy performance with impressive results, including an output voltage of 2.26 mV, a current density of 0.18 nA/cm^2, and a power output of 0.51 pW at 75% RH. According to the study, excessive hydrophilicity causes water molecules to adsorb quickly, which slows down device recovery, while insufficient hydrophilicity causes slow adsorption and hence sluggish device response. Therefore, to develop a humidity-to-energy device with improved response and recovery performance, future research should focus on optimizing factors to achieve an optimal level of hydrophilicity that neither absorbs water molecules too rapidly nor too slowly, thereby enhancing device performance.

Acknowledgement

The Ministry of Higher Education Malaysia and the School of Electrical Engineering, College of Engineering, UiTM Shah Alam are acknowledged by the authors for their support in this research. Funding for this project is provided by the Fundamental Research Grant Scheme (FRGS) (FRGS/1/2022/TK07/UITM/02/7).

Conflict of Interest

Authors declare that there is no conflict of interest regarding the publication of the paper.

Author Contribution

The authors confirm contribution to the paper as follows: ***study conception and design:*** Mohamad Hafiz Mamat, *Mohd Khairul Ahmad, Suriani Abu Bakar;* ***data collection:*** *Nurul Syafiqah Mohamed Mustakim, Dayana Kamaruzaman;* ***analysis and interpretation of results:*** *Mohd Firdaus Malek, Mohd Hanapiah Abdullah, Norfarariyanti Parimon, Nagamalai Vasimalai;* ***draft manuscript preparation:*** *Nurul Syafiqah Mohamed Mustakim,* Mohamad Hafiz Mamat, *A Shamsul Rahimi A Subki. All authors reviewed the results and approved the final version of the manuscript.*

References

[1] Kapilan, N., Nithin, K. C., & Chiranth, K. N. (2022). Challenges and opportunities in solar photovoltaic system. *Materials Today: Proceedings*, *62*, 3538-3543, https://doi.org/https://doi.org/10.1016/j.matpr.2022.04.390

[2] Mohamed Mustakim, N. S., Ubani, C. A., Sepeai, S., Ahmad Ludin, N., Mat Teridi, M. A., & Ibrahim, M. A. (2018). Quantum dots processed by SILAR for solar cell applications. *Solar Energy*, *163*, 256-270, https://doi.org/https://doi.org/10.1016/j.solener.2018.02.003

[3] Hayat, M. B., Ali, D., Monyake, K. C., Alagha, L., & Ahmed, N. (2019). Solar energy—A look into power generation, challenges, and a solar-powered future. *International Journal of Energy Research*, *43*(3), 1049-1067, https://doi.org/https://doi.org/10.1002/er.4252

[4] Mustakim, N. S. M., Sepeai, S., Ludin, N. A., Mat Teridi, M. A., & Ibrahim, M. A. (2019). Properties of Nanostructured Rutile Titanium Dioxide (TiO2) Thin Film Deposited with Silver Sulfide (Ag2S) Quantum Dots as Photoanode for Solar Photovoltaic. *Solid State Phenomena*, *290*, 329-335, https://doi.org/10.4028/www.scientific.net/SSP.290.329

[5] Mustakim, N. S., Sepeai, S., Ludin, N. A., Teridi, M. A. M., & Ibrahim, M. A. (2020). Effect of silver sulphide (Ag2S) layer towards the performance of copper indium sulphide (CuInS2) quantum dots sensitised solar cell. *International Journal of Nanotechnology*, *17*(11-12), 795-806, https://doi.org/10.1504/ijnt.2020.112383

[6] Joshi, G., Pandey, J. K., Rana, S., & Rawat, D. S. (2017). Challenges and opportunities for the application of biofuel. *Renewable and Sustainable Energy Reviews*, *79*, 850-866, https://doi.org/https://doi.org/10.1016/j.rser.2017.05.185

[7] Qidwai, A., Shukla, S. K., Kumar, R., Pandey, A., & Dikshit, A. (2018). Introduction of Nanotechnology in the Field of Biofuel Production. In N. Srivastava, M. Srivastava, H. Pandey, P. K. Mishra, & P. W. Ramteke (Eds.), *Green Nanotechnology for Biofuel Production* (pp. 29-38). Springer International Publishing, https://doi.org/10.1007/978-3-319-75052-1_3

[8] Solarin, S. A., & Bello, M. O. (2022). Wind energy and sustainable electricity generation: evidence from Germany. *Environment, Development and Sustainability*, *24*(7), 9185-9198, https://doi.org/10.1007/s10668-021-01818-x

[9] Charabi, Y., & Abdul-Wahab, S. (2020). Wind turbine performance analysis for energy cost minimization. *Renewables: Wind, Water, and Solar*, *7*(1), 5, https://doi.org/10.1186/s40807-020-00062-7

[10] Agarwal, T., Verma, S., & Gaurh, A. (2016, 3-5 March 2016). Issues and challenges of wind energy. 2016 International Conference on Electrical, Electronics, and Optimization Techniques (ICEEOT),

[11] Chen, Z. (2023). Challenges and Perspectives of Wind Energy Technology. *Wind*, *3*(4), 545-547. https://www.mdpi.com/2674-032X/3/4/30

[12] Ma, M., Guo, L., Anderson, D. G., & Langer, R. (2013). Bio-Inspired Polymer Composite Actuator and Generator Driven by Water Gradients. *Science*, *339*(6116), 186-189, https://doi.org/10.1126/science.1230262

[13] Chen, X., Mahadevan, L., Driks, A., & Sahin, O. (2014). Bacillus spores as building blocks for stimuli-responsive materials and nanogenerators. *Nature Nanotechnology*, *9*(2), 137-141, https://doi.org/10.1038/nnano.2013.290

[14] Zhao, F., Cheng, H., Zhang, Z., Jiang, L., & Qu, L. (2015). Direct Power Generation from a Graphene Oxide Film under Moisture. *Advanced Materials*, *27*(29), 4351-4357, https://doi.org/https://doi.org/10.1002/adma.201501867

[15] Yan, H., Liu, Z., & Qi, R. (2022). A review of humidity gradient-based power generator: Devices, materials and mechanisms. *Nano Energy*, *101*, 107591, https://doi.org/https://doi.org/10.1016/j.nanoen.2022.107591

[16] Zhang, Y., Nandakumar, D. K., & Tan, S. C. (2020). Digestion of Ambient Humidity for Energy Generation. *Joule*, *4*(12), 2532-2536, https://doi.org/https://doi.org/10.1016/j.joule.2020.10.003

[17] Li, X., Guo, Y., Meng, J., Li, X., Li, M., & Gao, D. (2022). Self-Powered Carbon Ink/Filter Paper Flexible Humidity Sensor Based on Moisture-Induced Voltage Generation. *Langmuir*, *38*(27), 8232-8240, https://doi.org/10.1021/acs.langmuir.2c00566

[18] Zhao, H., Tang, Z., He, M., Yang, X., Lai, S., An, K., Han, S., Qu, Z., Zhou, W., & Wang, Z. (2023). Effect of oxygen functional groups on competitive adsorption of benzene and water on carbon materials: Density functional theory study. *Science of The Total Environment*, *863*, 160772, https://doi.org/https://doi.org/10.1016/j.scitotenv.2022.160772

[19] Kamaruzaman, D., Mohamed Mustakim, N. S., A Subki, A. S. R., Parimon, N., Yaakob, M. K., Malek, M. F., Vasimalai, N., Abdullah, M. H., Abu Bakar, S., Ahmad, M. K., Thomas, S., & Mamat, M. H. (2024). Polystyrene Waste-ZnO nanocomposite film for energy harvesting via hydrophobic triboelectric nanogenerator: Transforming waste into energy. *Materials Today Sustainability*, *26*, 100726, https://doi.org/https://doi.org/10.1016/j.mtsust.2024.100726

[20] Hosseini, S., Savaloni, H., & Gholipour Shahraki, M. (2019). Influence of surface morphology and nano-structure on hydrophobicity: A molecular dynamics approach. *Applied Surface Science*, *485*, 536-546, https://doi.org/10.1016/j.apsusc.2019.04.236

[21] Nundy, S., Ghosh, A., & Mallick, T. K. (2020). Hydrophilic and Superhydrophilic Self-Cleaning Coatings by Morphologically Varying ZnO Microstructures for Photovoltaic and Glazing Applications. *ACS Omega*, *5*(2), 1033-1039, https://doi.org/10.1021/acsomega.9b02758

[22] Riveiro, A., Maçon, A. L. B., del Val, J., Comesaña, R., & Pou, J. (2018). Laser Surface Texturing of Polymers for Biomedical Applications [Review]. *Frontiers in Physics*, *6*, https://doi.org/10.3389/fphy.2018.00016

[23] Berhe, M. G., & Gebreslassie, Y. T. (2023). Biomedical Applications of Biosynthesized Nickel Oxide Nanoparticles. *International Journal of Nanomedicine*, *18*(null), 4229-4251, https://doi.org/10.2147/IJN.S410668

[24] Bokov, D., Turki Jalil, A., Chupradit, S., Suksatan, W., Javed Ansari, M., Shewael, I. H., Valiev, G. H., & Kianfar, E. (2021). Nanomaterial by Sol-Gel Method: Synthesis and Application. *Advances in Materials Science and Engineering*, *2021*(1), 5102014, https://doi.org/https://doi.org/10.1155/2021/5102014

[25] Parimon, N., Mamat, M.H., Suriani, A.B., Mohamed, A., Ahmad, M.K., Banu, I.S., Vasimalai, N. and Rusop, M., 2021. Physical properties of novel α-Fe2O3/NiO heterostructures through immersion/sol–gel spin coating method: different deposition numbers of NiO layer. *Jurnal Teknologi*, *83*(5), pp.19-26. https://doi.org/10.11113/jurnalteknologi.v83.16793

[26] Parimon, N., Mamat, M. H., Shameem Banu, I. B., Vasimalai, N., Suriani, A. B., Mohamed, A., Ahmad, M. K., & Rusop, M. (2021). Influence of Doping Concentration on the Zinc Doped Nickel Oxide Nanostructures: Morphological, Structural, and Optical Properties. *IOP Conference Series: Earth and Environmental Science*, *682*(1), 012070, https://doi.org/10.1088/1755-1315/682/1/012070

[27] Catania, F., Marras, E., Giorcelli, M., Jagdale, P., Lavagna, L., Tagliaferro, A., & Bartoli, M. (2021). A Review on Recent Advancements of Graphene and Graphene-Related Materials in Biological Applications. *Applied Sciences*, *11*(2), 614, https://www.mdpi.com/2076-3417/11/2/614

[28] Mouchou, R. T., Ukoba, K. O., Laseinde, O. T., & Jen, T. C. (2021). Fabrication of p-NiO/n-TiO2 Solar Device for Photovoltaic Application. *International Journal of Photoenergy*, *2021*(1), 1214170, https://doi.org/https://doi.org/10.1155/2021/1214170

[29] Suragtkhuu, S., Sunderiya, S., Myagmarsereejid, P., Purevdorj, S., Bati, A. S. R., Bold, B., Zhong, Y. L., Davaasambuu, S., & Batmunkh, M. (2023). Graphene-Like Monoelemental 2D Materials for Perovskite Solar Cells. *Advanced Energy Materials*, *13*(12), 2204074, https://doi.org/https://doi.org/10.1002/aenm.202204074

[30] Deji, R., Rahul, Choudhary, B. C., & Sharma, R. K. (2023). Role of Graphene-Based Materials in Gas Sensing Applications: From Synthesis to Device Fabrication. In A. N. Grace, P. Sonar, P. Bhardwaj, & A. Chakravorty (Eds.), *Handbook of Porous Carbon Materials* (pp. 493-518). Springer Nature Singapore, https://doi.org/10.1007/978-981-19-7188-4_18

[31] Li, Q., Zeng, W., & Li, Y. (2022). NiO-Based Gas Sensors for Ethanol Detection: Recent Progress. *Journal of Sensors*, *2022*(1), 1855493, https://doi.org/https://doi.org/10.1155/2022/1855493

[32] Mokoena, T. P., Swart, H. C., & Motaung, D. E. (2019). A review on recent progress of p-type nickel oxide based gas sensors: Future perspectives. *Journal of Alloys and Compounds*, *805*, 267-294, https://doi.org/https://doi.org/10.1016/j.jallcom.2019.06.329

[33] Subki, A. S. R. A., Mamat, M. H., Musa, M. Z., Abdullah, M. H., Shameem Banu, I. B., Vasimalai, N., Ahmad, M. K., Nafarizal, N., Suriani, A. B., Mohamad, A., Birowosuto, M. D., & Rusop, M. (2022). Effects of varying the amount of reduced graphene oxide loading on the humidity sensing performance of zinc oxide/reduced graphene oxide nanocomposites on cellulose filter paper. *Journal of Alloys and Compounds*, *926*, 166728, https://doi.org/https://doi.org/10.1016/j.jallcom.2022.166728

[34] Parimon, N., Mamat, M., Banu, I. S., Vasimalai, N., Ahmad, M., Suriani, A., Mohamed, A., & Rusop, M. (2021). Annealing temperature dependency of structural, optical and electrical characteristics of manganese-doped nickel oxide nanosheet array films for humidity sensing applications. *Nanomaterials and Nanotechnology*, *11*, 1847980420982788, https://doi.org/10.1177/1847980420982788

[35] Xu, W., Zhang, J., Li, Y., Zhang, L., Chen, L., Zhu, D., Cao, P., Liu, W., Han, S., Liu, X., & Lu, Y. (2019). p-Type transparent amorphous oxide thin-film transistors using low-temperature solution-processed nickel oxide. *Journal of Alloys and Compounds*, *806*, 40-51. https://doi.org/https://doi.org/10.1016/j.jallcom.2019.07.108

[36] Yuvaraja, S., Khandelwal, V., Krishna, S., Lu, Y., Liu, Z., Kumar, M., Tang, X., Maciel García, G. I., Chettri, D., Liao, C.-H., & Li, X. (2024). Enhancement-Mode Ambipolar Thin-Film Transistors and CMOS Logic Circuits using Bilayer Ga2O3/NiO Semiconductors. *ACS Applied Materials & Interfaces*, *16*(5), 6088-6097, https://doi.org/10.1021/acsami.3c15778

[37] Liu, L., Liu, Y., & Duan, X. (2020). Graphene-based vertical thin film transistors. *Science China Information Sciences*, *63*(10), 201401, https://doi.org/10.1007/s11432-020-2806-8

[38] Kim, H., Zhao, H. L., & van der Zande, A. M. (2024). Stretchable Thin-Film Transistors Based on Wrinkled Graphene and MoS2 Heterostructures. *Nano Letters*, *24*(4), 1454-1461, https://doi.org/10.1021/acs.nanolett.3c05091

[39] Baskoro, F., Wong, C.-B., Kumar, S. R., Chang, C.-W., Chen, C.-H., Chen, D. W., & Lue, S. J. (2018). Graphene oxide-cation interaction: Inter-layer spacing and zeta potential changes in response to various salt solutions. *Journal of Membrane Science*, *554*, 253-263, https://doi.org/https://doi.org/10.1016/j.memsci.2018.03.006

[40] Silambarasan, K., Archana, J., Athithya, S., Harish, S., Sankar Ganesh, R., Navaneethan, M., Ponnusamy, S., Muthamizhchelvan, C., Hara, K., & Hayakawa, Y. (2020). Hierarchical NiO@NiS@graphene nanocomposite as a sustainable counter electrode for Pt free dye-sensitized solar cell. *Applied Surface Science*, *501*, 144010, https://doi.org/https://doi.org/10.1016/j.apsusc.2019.144010

[41] Mahmoudi, T., Wang, Y., & Hahn, Y.-B. (2021). Highly stable perovskite solar cells based on perovskite/NiO-graphene composites and NiO interface with 25.9 mA/cm2 photocurrent density and 20.8% efficiency. *Nano Energy*, *79*, 105452, https://doi.org/https://doi.org/10.1016/j.nanoen.2020.105452

[42] Sankar, A., Chitra, S. V., Jayashree, M., Parthibavarman, M., & Amirthavarshini, T. (2022). NiO nanoparticles/graphene nanocomposite as high-performance pseudocapacitor electrodes: Design and implementation. *Diamond and Related Materials*, *122*, 108804, https://doi.org/https://doi.org/10.1016/j.diamond.2021.108804

[43] Sethi, M., Shenoy, U. S., & Bhat, D. K. (2021). Simple solvothermal synthesis of porous graphene-NiO nanocomposites with high cyclic stability for supercapacitor application. *Journal of Alloys and Compounds*, *854*, 157190, https://doi.org/https://doi.org/10.1016/j.jallcom.2020.157190

[44] Sahoo, G., Polaki, S. R., Pazhedath, A., Krishna, N. G., Mathews, T., & Kamruddin, M. (2021). Synergetic Effect of NiOx Decoration and Oxygen Plasma Treatment on Electrochemical Capacitor Performance of Vertical Graphene Nanosheets. *ACS Applied Energy Materials*, *4*(1), 791-800, https://doi.org/10.1021/acsaem.0c02683

[45] Zito, C. A., Perfecto, T. M., Fonseca, C. S., & Volanti, D. P. (2018). Effective reduced graphene oxide sheets/hierarchical flower-like NiO composites for methanol sensing under high humidity. *New Journal of Chemistry*, *42*(11), 8638-8645, https://doi.org/10.1039/c8nj01061g

[46] Thamer, B. M., Al-aizari, F. A., & Hameed, M. M. A. (2023). Zero-valent Ni/NiO core-shell nanosheets supported on graphene for highly efficient dye adsorption: Isotherm, kinetic and thermodynamic study. *Chemical Engineering Research and Design*, *197*, 656-668, https://doi.org/https://doi.org/10.1016/j.cherd.2023.08.023

[47] Sun, Z., Wen, X., Wang, L., Ji, D., Qin, X., Yu, J., & Ramakrishna, S. (2022). Emerging design principles, materials, and applications for moisture-enabled electric generation. *eScience*, *2*(1), 32-46, https://doi.org/10.1016/j.esci.2021.12.009

[48] Chatterjee, S., Maiti, R., Miah, M., Saha, S. K., & Chakravorty, D. (2017). NiO Nanoparticle Synthesis Using a Triblock Copolymer: Enhanced Magnetization and High Specific Capacitance of Electrodes Prepared from the Powder. *ACS Omega*, *2*(1), 283-289, https://doi.org/10.1021/acsomega.6b00384

[49] Zhao, K., Lee, J. W., Yu, Z. G., Jiang, W., Oh, J. W., Kim, G., Han, H., Kim, Y., Lee, K., Lee, S., Kim, H., Kim, T., Lee, C. E., Lee, H., Jang, J., Park, J. W., Zhang, Y.-W., & Park, C. (2023). Humidity-Tolerant Moisture-Driven Energy Generator with MXene Aerogel–Organohydrogel Bilayer. *ACS Nano*, *17*(6), 5472-5485, https://doi.org/10.1021/acsnano.2c10747

[50] Ren, G., Wang, Z., Zhang, B., Liu, X., Ye, J., Hu, Q., & Zhou, S. (2021). A facile and sustainable hygroelectric generator using whole-cell Geobacter sulfurreducens. *Nano Energy*, *89*, 106361, https://doi.org/https://doi.org/10.1016/j.nanoen.2021.106361

[51] Ding, T., Liu, K., Li, J., Xue, G., Chen, Q., Huang, L., Hu, B., & Zhou, J. (2017). All-Printed Porous Carbon Film for Electricity Generation from Evaporation-Driven Water Flow. *Advanced Functional Materials*, *27*(22), 1700551, https://doi.org/https://doi.org/10.1002/adfm.201700551

[52] Shen, D., Xiao, M., Zou, G., Liu, L., Duley, W. W., & Zhou, Y. N. (2018). Self-Powered Wearable Electronics Based on Moisture Enabled Electricity Generation. *Advanced Materials*, *30*(18), 1705925, https://doi.org/https://doi.org/10.1002/adma.201705925

[53] Cheng, H., Huang, Y., Zhao, F., Yang, C., Zhang, P., Jiang, L., Shi, G., & Qu, L. (2018). Spontaneous power source in ambient air of a well-directionally reduced graphene oxide bulk [10.1039/C8EE01502C]. *Energy & Environmental Science*, *11*(10), 2839-2845, https://doi.org/10.1039/C8EE01502C

[54] Huang, Y., Cheng, H., Yang, C., Zhang, P., Liao, Q., Yao, H., Shi, G., & Qu, L. (2018). Interface-mediated hygroelectric generator with an output voltage approaching 1.5 volts. *Nature Communications*, *9*(1), 4166, https://doi.org/10.1038/s41467-018-06633-z

[55] Shi, S.-C., & Peng, Y.-Q. (2021). Hydrophobicity and Macroscale Tribology Behavior of Stearic Acid/Hydroxypropyl Methylcellulose Dual-Layer Composite. *Materials*, *14*(24), 7707, https://www.mdpi.com/1996-1944/14/24/7707

[56] Khairnar, S. D., & Shrivastava, V. S. (2019). Facile synthesis of nickel oxide nanoparticles for the degradation of Methylene blue and Rhodamine B dye: a comparative study. *Journal of Taibah University for Science*, *13*(1), 1108-1118, https://doi.org/10.1080/16583655.2019.1686248

[57] Arfaoui, M. A., Dolez, P. I., Dubé, M., & David, É. (2019). Preparation of a hydrophobic recycled jute-based nonwoven using a titanium dioxide/stearic acid coating. *The Journal of The Textile Institute*, *110*(1), 16-25. https://doi.org/10.1080/00405000.2018.1455313

[58] Batakliev, T., Petrova-Doycheva, I., Angelov, V., Georgiev, V., Ivanov, E., Kotsilkova, R., Casa, M., Cirillo, C., Adami, R., Sarno, M., & Ciambelli, P. (2019). Effects of Graphene Nanoplatelets and Multiwall Carbon Nanotubes on the Structure and Mechanical Properties of Poly(lactic acid) Composites: A Comparative Study. *Applied Sciences*, *9*(3), 469, https://www.mdpi.com/2076-3417/9/3/469

[59] Chen, G.-J., Lin, C.-M., Shih, Y.-H., & Jian, S.-R. (2022). The Microstructures and Characteristics of NiO Films: Effects of Substrate Temperature. *Micromachines*, *13*(11), 1940, https://www.mdpi.com/2072-666X/13/11/1940

[60] Bayati, R., Molaei, R., Richmond, A., Nori, S., Wu, F., Kumar, D., Narayan, J., Reynolds, J. G., & Reynolds, C. L., Jr. (2014). Modification of properties of yttria stabilized zirconia epitaxial thin films by excimer laser annealing. *ACS Appl Mater Interfaces*, *6*(24), 22316-22325, https://doi.org/10.1021/am506298y